

Importance of magnetic shape anisotropy in determining magnetic and electronic properties of monolayer VSi₂P₄

San-Dong Guo¹, Yu-Ling Tao¹, Kai Cheng¹, Bing Wang² and Yee-Sin Ang³

¹*School of Electronic Engineering, Xi'an University of Posts and Telecommunications, Xi'an 710121, China*

²*Institute for Computational Materials Science, School of Physics and Electronics, Henan University, 475004, Kaifeng, China and*

³*Science, Mathematics and Technology (SMT), Singapore University of Technology and Design (SUTD), 8 Somapah Road, Singapore 487372, Singapore*

Two-dimensional (2D) ferromagnets have been a fascinating subject of research, and magnetic anisotropy (MA) is indispensable for stabilizing the 2D magnetic order. Here, we investigate magnetic anisotropy energy (MAE), magnetic and electronic properties of VSi₂P₄ by using the generalized gradient approximation plus U (GGA+ U) approach. For large U , the magnetic shape anisotropy (MSA) energy has a more pronounced contribution to the MAE, which can overcome the magnetocrystalline anisotropy (MCA) energy to evince an easy-plane. For fixed out-of-plane MA, monolayer VSi₂P₄ undergoes ferrovalley (FV), half-valley-metal (HVM), valley-polarized quantum anomalous Hall insulator (VQAHI), HVM and FV states with increasing U . However, for assumptive in-plane MA, there is no special quantum anomalous Hall (QAH) state and spontaneous valley polarization within considered U range. According to the MAE and electronic structure with fixed out-of-plane or in-plane MA, the intrinsic phase diagram shows common magnetic semiconductor (CMS), FV and VQAHI in monolayer VSi₂P₄. At representative $U=3$ eV widely used in references, VSi₂P₄ can be regarded as a 2D- XY magnet, not Ising-like 2D long-range order magnets predicted in previous works with only considering MCA energy. Our findings shed light on importance of MSA in determining magnetic and electronic properties of monolayer VSi₂P₄.

Keywords: Magnetic anisotropy, 2D ferromagnets, Phase transition

Email:sandongyuwang@163.com

I. INTRODUCTION

There has been a tremendous interest in searching 2D magnetic materials, which can interplay with other important properties of materials such as FV, ferroelectricity, piezoelectricity and QAH effects. According to the Mermin-Wagner theorem, the long-range magnetic order at finite temperature for the 2D isotropic Heisenberg spin systems is prohibited¹. Experimentally, both the CrI₃ monolayer and Cr₂Ge₂Te₆ bilayer show an easy out-of-plane magnetization^{2,3}, while the 2D magnet CrCl₃ has an easy in-plane magnetization^{4,5}. The underlying mechanism is that MA is responsible for the stable 2D magnetic order. With the presence of out-of-plane magnetization, the long-range FM order can sustain at finite temperature by opening a magnon gap to resist thermal agitations⁶. An easy-plane anisotropy can realize the quasi-ordered topological vortex/antivortex pairs, which can be described by the Berezinskii-Kosterlitz-Thouless (BKT) theory based on the 2D XY model⁷. Moreover, MA can affect the symmetry of 2D systems, and then produce important influence on their topological and valley properties⁸⁻¹¹, when the spin-orbital coupling (SOC) is included. For these 2D systems, the FV and QAH states can exist with fixed out-of-plane magnetic anisotropy, but these special states disappear for in-plane case⁹⁻¹¹.

The magnetization direction can be determined by MAE, which mainly include MCA and MSA energies. Compared with SOC-induced MCA, the MSA due to the magnetic dipole-dipole (D-D) interaction is often relatively weak and is neglected. But for a 2D system with weak MCA, the MSA may have an important con-

tribution. The representative example is 2D magnet CrCl₃, which has been confirmed to have an easy in-plane magnetization in experiment^{4,5}. When only considering MCA energy, the CrCl₃ shows an easy out-of-plane magnetization, which is contrary to experimental results¹². When including MSA energy, the theoretical results agree well with experimental in-plane magnetization¹². Another case is CrSBr monolayer¹³. The MCA energy shows that the b axis is the easy one, and the a axis would be hard. When including MSA energy, the MAE gives the easy magnetization b axis and hard c axis.

Recently, the septuple-atomic-layer 2D MoSi₂N₄ and WSi₂N₄ have been successfully synthesized by the chemical vapor deposition method¹⁴. Subsequently, 2D MA₂Z₄ family with a septuple-atomic-layer structure has been established, which possess emerging topological, magnetic, valley and superconducting properties¹⁵. The VA₂Z₄ of them possess magnetic properties, which have been widely investigated^{9,16-21} due to their FV properties. The monolayer VSi₂P₄ is a typical example, which is predicted to have out-of-plane magnetization with only considering MCA energy (6.38 μ eV)¹⁷. In recent works, the Janus monolayer VSiGeN₄ is predicted to be in-plane magnetization with only considering MCA energy, and the in-plane magnetization is enhanced, when including MSA energy (about -17 μ eV)^{18,21}. This implies that VSi₂P₄ may be an in-plane 2D XY magnet without the long-range FM order. In this work, we investigate MCA energy, MSA energy, MAE and electronic structures of VSi₂P₄ as a function of U , and reveal the importance of MSA in determining its magnetic, topological and valley properties. At representative $U=3$ eV^{9,15-21}, VSi₂P₄

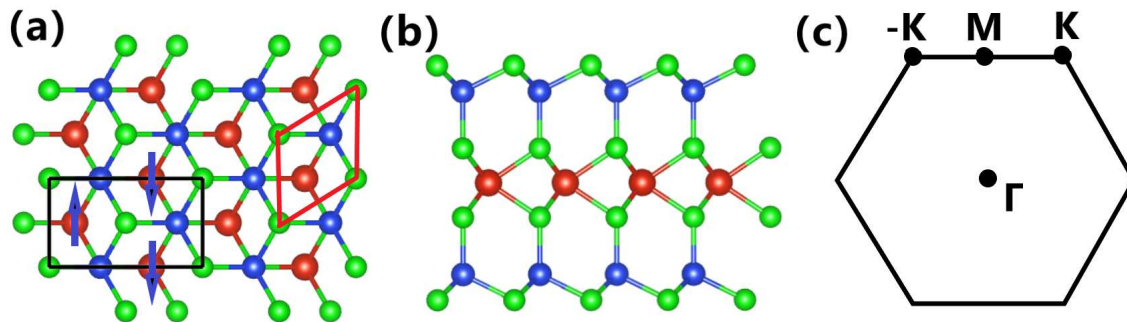


FIG. 1. (Color online) For VSi_2P_4 monolayer, (a): top view and (b): side view of crystal structure. The primitive (rectangle supercell) cell is shown by red (black) lines, and the AFM configuration is marked with blue arrows in (a). (c): the first BZ with high symmetry points.

can be regarded as a 2D-XY magnet, which is different from previous conclusion that the Ising-like 2D long-range order magnet is predicted with only considering MCA energy^{9,17}.

The rest of the paper is organized as follows. In the next section, we shall give our computational details and methods. In the next few sections, we shall present structure and MAE, and electronic structures of VSi_2P_4 monolayer. Finally, we shall give our conclusion.

II. COMPUTATIONAL DETAIL

Based on density-functional theory (DFT)²², the spin-polarized first-principles calculations are performed by employing the projected augmented wave method, as implemented in VASP code^{23–25}. We use popular generalized gradient approximation of Perdew-Burke-Ernzerhof (PBE-GGA)²⁶ as exchange-correlation functional. To consider on-site Coulomb correlation of V atoms, the GGA+ U method is used within the rotationally invariant approach proposed by Dudarev et al²⁷. To attain accurate results, we use the energy cut-off of 500 eV, total energy convergence criterion of 10^{-8} eV and force convergence criteria of less than $0.0001 \text{ eV} \cdot \text{\AA}^{-1}$ on each atom. A vacuum space of more than 32 \AA is used to avoid the interactions between the neighboring slabs. We use Γ -centered $15 \times 15 \times 1$ k-point meshes in the Brillouin zone (BZ) for structure optimization and electronic structures calculations, and $9 \times 16 \times 1$ Monkhorst-Pack k-point meshes for calculating ferromagnetic (FM)/antiferromagnetic (AFM) energy with rectangle supercell. The SOC effect is explicitly included to investigate MCA, electronic and topological properties of VSi_2P_4 monolayer. The Berry curvatures are calculated directly from wave functions based on Fukui's method²⁸, as implemented in VASPBERRY code^{29,30}. The mostly localized Wannier functions are constructed from the d -orbitals of V atom, s - and p -orbitals of Si and Ge, p -orbitals of N atoms by Wannier90 code³¹, and then edge states are calculated by employing the WannierTools package³².

III. STRUCTURE AND MAGNETIC ANISOTROPY ENERGY

The crystal structures of monolayer VSi_2P_4 are plotted in Figure 1, along with the first BZ with high-symmetry points. The primitive cell contains one V, two Si, and four P atoms, which is stacked by seven atomic layers of P-Si-P-V-P-Si-P. Each V atom is coordinated with six P atoms, which forms a trigonal prismatic configuration. In other words, this VP_2 layer is sandwiched by two Si-P bilayers, and the crystal symmetry of VSi_2P_4 is $P\bar{6}m2$ (No.187) with broken inversion symmetry. The optimized lattice constants a of VSi_2P_4 monolayer is 3.486 \AA , agreeing well with previous theoretical value⁹.

Based on Goodenough-Kanamori-Anderson rules^{33,34}, the superexchange coupling between two V atoms is FM, because the V-P-V bonding angle is 91.68° , which is close to 90° . To confirm this, the energy differences (per formula unit) between AFM and FM ordering as a function of U are also plotted in FIG.1 of electronic supplementary information (ESI). Calculated results show that the FM state is always the magnetic ground state of VSi_2P_4 within considered U range. It is found that energy difference between AFM and FM ordering around $U=1.45 \text{ eV}$ has a sudden jump, which is due to abrupt change of magnetic moment of V atom for AFM ordering (The magnetic moment of V atom changes from $0.74 \mu_B$ to $0 \mu_B$ to $0.079 \mu_B$ to $0.81 \mu_B$, when U varies from 1.3 eV to 1.4 eV to 1.5 eV to 1.6 eV), and the small magnetic moment of V atom reduces the magnetic interaction energy. Similar phenomenon can be observed, when energy difference between AFM and FM ordering is as a function of strain for VSiGeN_4 and VSi_2P_4 ^{17,21}.

The orientation of magnetization plays an important role on magnetic and electronic states of some 2D materials^{8–11}. The MAE can be used to measure the dependence of the energy on the orientation of magnetization. The MAE originates mainly from two parts: (1) MCA energy E_{MCA} , which is an intrinsic property of the material caused by the SOC; (2) MSA energy E_{MSA} ,

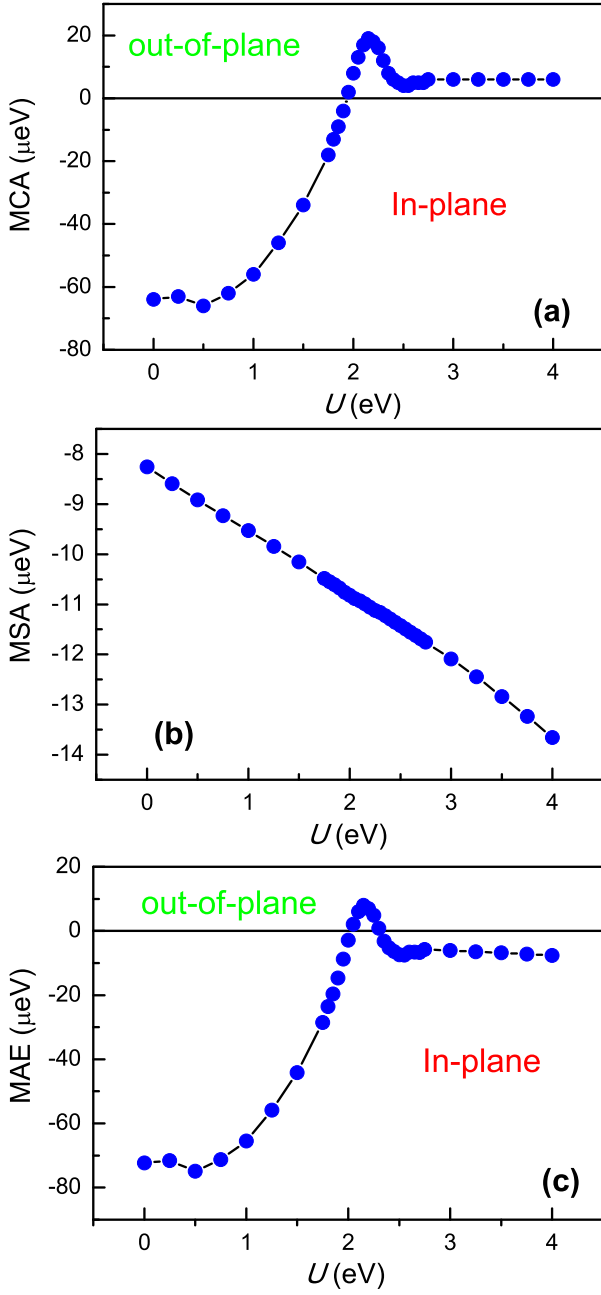


FIG. 2. (Color online) For VSi₂P₄ monolayer, MCA energy (a), MSA energy (b) and MAE (c) as a function of U .

which is basically the anisotropic D-D interaction^{12,13}:

$$E_{D-D} = \frac{1}{2} \frac{\mu_0}{4\pi} \sum_{i \neq j} \frac{1}{r_{ij}^3} [\vec{M}_i \cdot \vec{M}_j - \frac{3}{r_{ij}^2} (\vec{M}_i \cdot \vec{r}_{ij})(\vec{M}_j \cdot \vec{r}_{ij})] \quad (1)$$

where the \vec{M}_i represents the local magnetic moments and \vec{r}_{ij} are vectors that connect the sites i and j . For the monolayer with a collinear FM, when the spins lie in the

plane, the Equation 1 can be written as:

$$E_{D-D}^{\parallel} = \frac{1}{2} \frac{\mu_0 M^2}{4\pi} \sum_{i \neq j} \frac{1}{r_{ij}^3} [1 - 3 \cos^2 \theta_{ij}] \quad (2)$$

where θ_{ij} is the angle between the \vec{M} and \vec{r}_{ij} . When the spins are out of plane ($\theta_{ij}=90^\circ$), the Equation 1 can further be simplified as:

$$E_{D-D}^{\perp} = \frac{1}{2} \frac{\mu_0 M^2}{4\pi} \sum_{i \neq j} \frac{1}{r_{ij}^3} \quad (3)$$

The E_{MSA} ($E_{D-D}^{\parallel} - E_{D-D}^{\perp}$) can be expressed as:

$$E_{MSA} = \frac{3}{2} \frac{\mu_0 M^2}{4\pi} \sum_{i \neq j} \frac{1}{r_{ij}^3} \cos^2 \theta_{ij} \quad (4)$$

The MSA tends to make magnetic moments of magnetic elements directed parallel to the surfaces, which can minimize magnetostatic energy. Usually, the MCA energy dominates the MAE, and MSA energy can be ignored. However, MSA becomes significant to MAE for materials with weak SOC.

Firstly, we calculate MCA energy by $E_{MCA} = E_{SOC}^{\parallel} - E_{SOC}^{\perp}$, which is obtained from GGA+U+SOC calculations. The E_{MCA} as a function of U is plotted in Figure 2 (a). Calculated results show multiple transitions in the MCA. With increasing U , the E_{MCA} changes from negative value to positive value, which means a transition from in-plane to out-of-plane. At $U=3.0$ eV, the calculated E_{MCA} (about 6 μeV) is consistent with available result (6.38 μeV)¹⁷. Secondly, we calculate MCA energy by Equation 4, which depends on the crystal structure and local magnetic moment of V (M_V). The M_V as a function of U is shown in FIG.2 of ESI. It is found that M_V increases (0.89 μ_B -1.15 μ_B) with increasing U . The E_{MSA} as a function of U is shown in Figure 2 (b), and the E_{MSA} changes from -8 μeV to -14 μeV , when U varies from 0 eV to 4 eV. Calculated results show that the MSA is in favour of in-plane anisotropy. Finally, the MAE can be obtained by $E_{MAE} = E_{MCA} + E_{MSA}$, which is plotted in Figure 2 (c). When U is between 2.03 eV and 2.31 eV, the positive MAE means a preferred out-of-plane polarization. When $U > 2.31$ eV and $U < 2.03$ eV, the in-plane anisotropy can be observed due to negative MAE.

For VA₂Z₄, the $U=3$ eV has been adopted in previous calculations^{9,15-21}. The VSi₂P₄ is predicted to be an out-of-plane ferromagnet (Ising-like 2D magnets) due to only considering MCA energy¹⁷. However, our calculated results show that VSi₂P₄ can be regarded as a 2D-XY magnet like the CrCl₃ monolayer^{4,5,12}. The in-plane easy magnetization means that there is no energetic barrier to the rotation of magnetization in the xy plane, and a BKT magnetic transition to a quasi-long-range phase can be observed at a critical temperature^{35,36}. The critical temperature $T_{BKT} = 1.335 \frac{J}{K_B}$ is obtained from the results of the Monte Carlo simulation for 2D-XY magnets on a

triangular lattice^{37,38}, where J is the nearest-neighboring exchange parameter and K_B is the Boltzmann constant. In a FM configuration, each V has six neighbors with the same spin, while, for AFM configuration, V has four neighbors with the opposite spin, and has two with the same spin. Based on the Heisenberg spin model, the FM (E_{FM}) and AFM (E_{AFM}) energy can be written as:

$$E_{FM} = E_0 - (6J + 2A)S^2 \quad (5)$$

$$E_{AFM} = E_0 + (2J - 2A)S^2 \quad (6)$$

where E_0 is the total energy of systems without magnetic coupling, and A means the easy-axis single-ion anisotropy. Hence, J can be obtained directly from the energy difference:

$$J = \frac{E_{AFM} - E_{FM}}{8S^2} \quad (7)$$

The calculated J is 16.07 meV ($S = \frac{1}{2}$) at $U=3$ eV, and the T_{BKT} is predicted to be 249 K.

IV. ELECTRONIC STRUCTURES

The magnetization is a pseudovector, which will lead to that the out-of-plane FM breaks all possible vertical mirror symmetry of the system, while preserves the horizontal mirror symmetry. The spontaneous valley polarization and a nonvanishing Chern number of 2D system can exist with the preserved horizontal mirror symmetry⁸. Thus, the MA of 2D system is very important to decide its electronic state. Firstly, the out-of-plane MA is fixed within considered U range. The energy band structures of VSi_2P_4 at some representative U values are plotted in FIG.3 of ESI. The evolutions of total energy band gap along with those at -K/K point and the valley splitting for both valence and conduction bands as a function of U are shown in Figure 3. Around about $U=2.20$ eV and 2.40 eV, the total energy band gap of VSi_2P_4 is closed, and the HVM state can be achieved³⁹, whose conduction electrons are intrinsically 100% valley polarized. At about $U=2.20$ eV (2.40 eV), the band gap of K (-K) valley gets closed, while a band gap at -K (K) valley is kept.

In a trigonal prismatic crystal field environment, the V- d orbitals split into low-lying d_z^2 orbital, $d_{xy}+d_{x^2-y^2}$ and $d_{xz}+d_{yz}$ orbitals. Calculated results show that $d_{x^2-y^2}+d_{xy}$ or d_z^2 orbitals of V atoms dominate K and -K valleys of both valence and conduction bands, and the V- d orbital characters energy band structures at representative $U=1.50$ eV, 2.25 eV and 3.00 eV are plotted in FIG.4 of ESI. For $U<2.20$ eV, the $d_{x^2-y^2}+d_{xy}/d_z^2$ orbitals dominate K and -K valleys of valence/conduction bands (For example $U=1.50$ eV). With increasing U between 2.20 eV and 2.40 eV, the band inversion between $d_{xy}+d_{x^2-y^2}$ and d_z^2 orbitals at K valley can be observed (For example $U=2.25$ eV), which is accompanied by the first HVM state. When U is larger than 2.40 eV, the

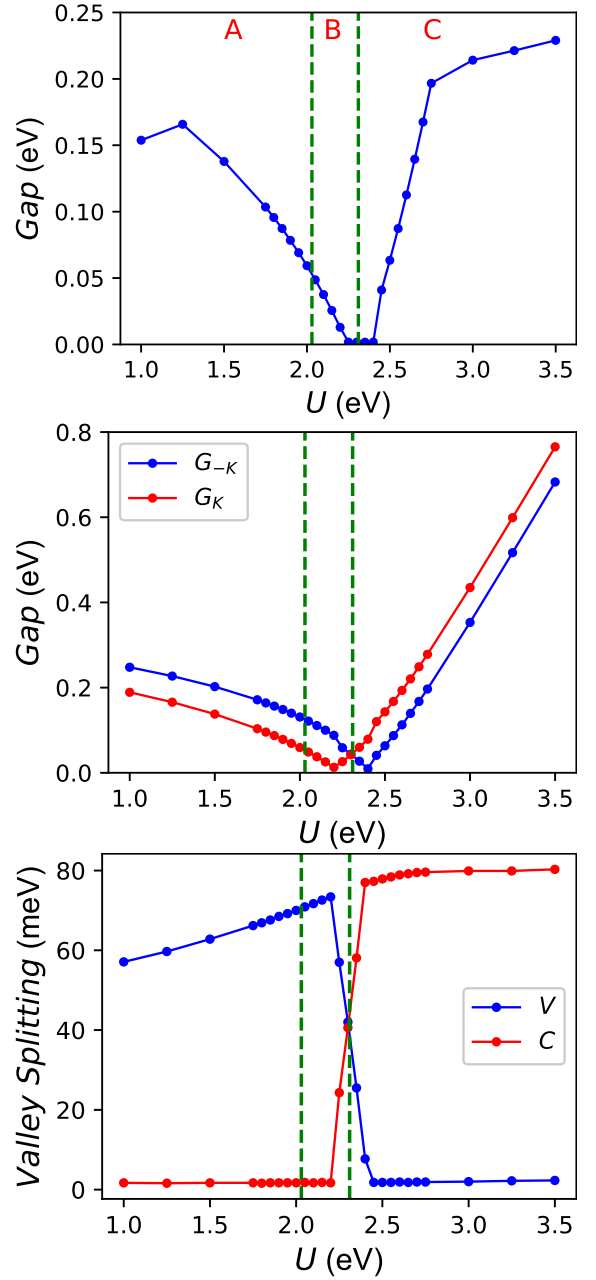


FIG. 3. (Color online) For VSi_2P_4 monolayer with fixed out-of-plane MA, Top panel: the global energy band gap; Middle panel: the energy band gaps for -K and K valleys; Bottom panel: the valley splitting for both valence and conduction bands as a function of U . The A and C regions mean in-plane, while the B region for out-of-plane.

band inversion between $d_{xy}+d_{x^2-y^2}$ and d_z^2 orbitals occurs at -K valley (For example $U=3.00$ eV), along with the second HVM state. These lead to that the distributions of $d_{x^2-y^2}+d_{xy}$ and d_z^2 orbitals of $0 \text{ eV} < U < 2.20$ eV are opposite to those of $2.40 \text{ eV} < U < 4$ eV.

The distributions of Berry curvature are calculated, and they are plotted in FIG.5 at representative $U=1.50$ eV, 2.25 eV and 3.00 eV. For $0 \text{ eV} < U < 2.20$ eV and 2.40

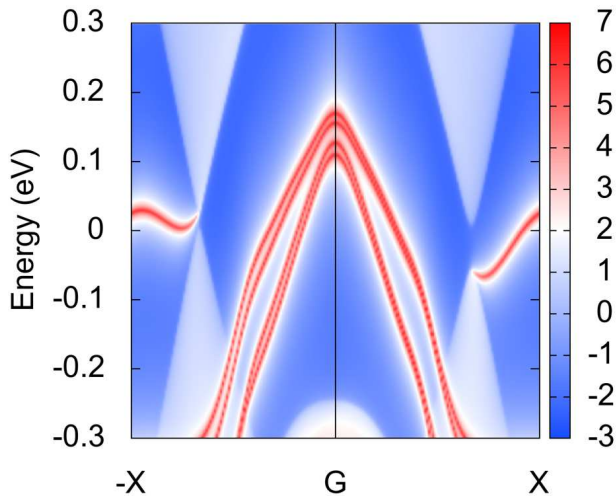


FIG. 4. (Color online) For VSi_2P_4 monolayer with out-of-plane MA, the topological edge states at representative $U=2.25$ eV.

$eV < U < 4$ eV, the opposite signs and different magnitudes for Berry curvatures can be observed around $-K$ and K valleys. However, for 2.20 eV $< U < 2.40$ eV, the Berry curvatures around $-K$ and K valleys show the same signs and different magnitudes. These indicate that the flipping of the sign of Berry curvature will occur at K or $-K$ valley. The positive Berry curvature (For example $U=1.50$ eV) changes into negative one (For example $U=2.25$ eV) at K valley, and then the negative Berry curvature (For example $U=2.25$ eV) changes into positive one (For example $U=3.00$ eV) at $-K$ valley. The twice flipping of the sign of Berry curvature is related with twice band inversion between $d_{xy}+d_{x^2-y^2}$ and d_{z^2} orbitals.

With increasing U , twice gap close, band inversion and flipping of the sign of Berry curvature suggest twice topological phase transition, and the QAH state may exist. To confirm this, the edge states and Chern number are calculated. Calculated results show that there are no nontrivial chiral edge states for 0 eV $< U < 2.20$ eV and 2.40 eV $< U < 4$ eV. When U is between 2.20 eV and 2.40 eV, the VSi_2P_4 is a QAH phase. The edge states at representative $U=2.25$ eV are plotted in Figure 4, which shows a nontrivial chiral edge state connecting the conduction bands and valence bands, implying a QAH phase. The predicted Chern number $C=-1$ by integrating the Berry curvature within the first BZ.

For 0 eV $< U < 2.20$ eV, the valley splitting of valence band is observable, while the valley splitting of conduction band can be ignored. However, for 2.40 eV $< U < 4$ eV, the opposite situation can be observed with respect to the case of 0 eV $< U < 2.20$ eV. For 2.20 eV $< U < 2.40$ eV, the valley splitting of valence/condition bands decreases/increases from observable/ignored value to ignored/observable one with increasing U . In this region, VSi_2P_4 is a VQAH with spontaneous valley splitting and chiral edge states. These can be understood by the distributions of $d_{x^2-y^2}+d_{xy}$ and d_{z^2} orbitals. If

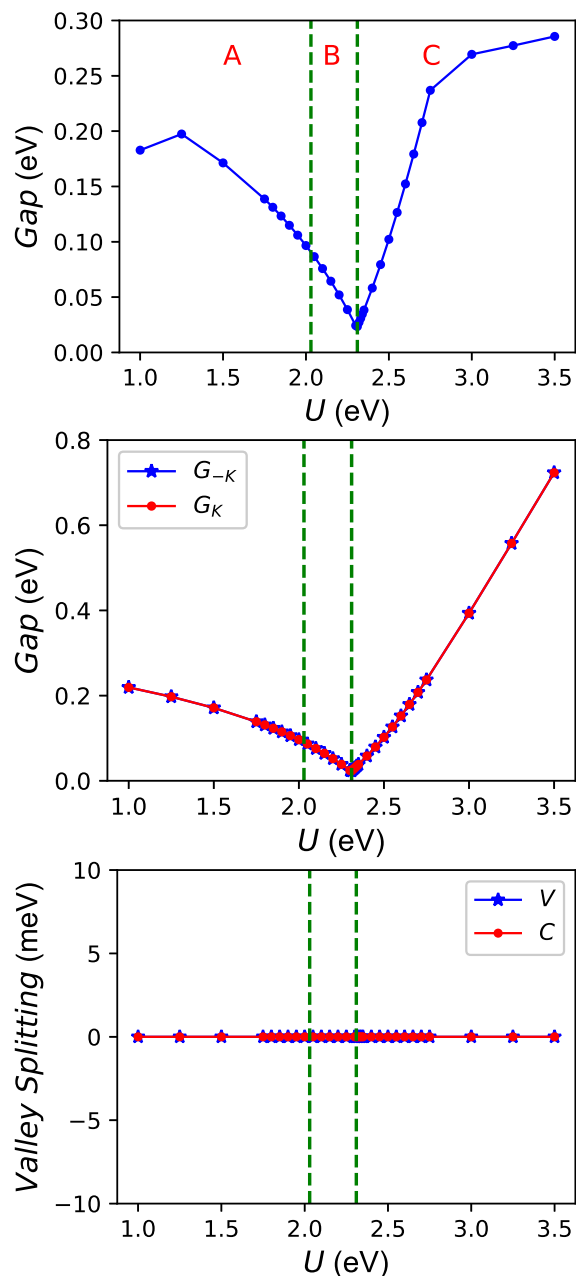


FIG. 5. (Color online) For VSi_2P_4 monolayer with fixed in-plane MA, Top panel: the global energy band gap; Middle panel: the energy band gaps for $-K$ and K valleys; Bottom panel: the valley splitting for both valence and conduction bands as a function of U . The A and C regions mean in-plane, while the B region for out-of-plane.

$d_{x^2-y^2}+d_{xy}/d_{z^2}$ orbitals dominate $-K$ and K valleys, the valley splitting will be observable/ignored. The SOC Hamiltonian only involving the interaction of the same spin states mainly contributes to valley polarization, which with out-of-plane magnetization can be simplified as⁴⁰⁻⁴²:

$$\hat{H}_{SOC}^0 = \alpha \hat{L}_z \quad (8)$$

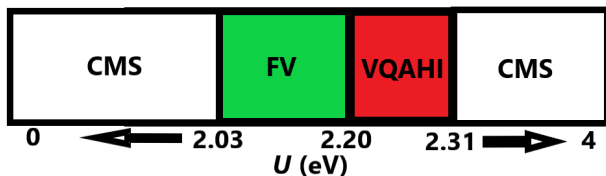


FIG. 6. (Color online) The phase diagram for monolayer VSi_2P_4 with different U values, including CMS, FV and VQAH.

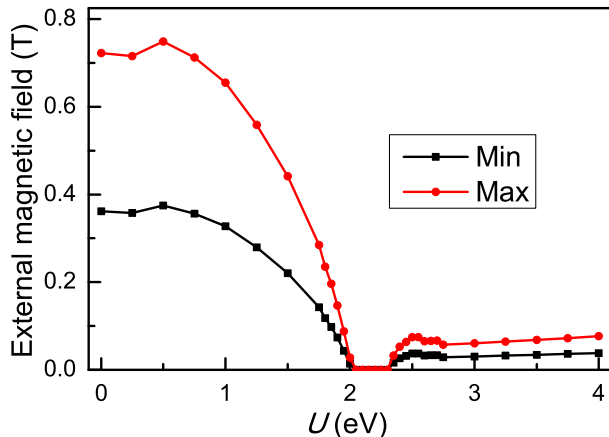


FIG. 7. (Color online) The external magnetic field range to overcome energy barrier from in-plane to out-of-plane as a function of U .

where \hat{L}_z/α is to the z component of orbital angular momenta/coupling strength. For $d_{x^2-y^2}+d_{xy}$ and d_{z^2} orbitals and the wave vector symmetry at the K and -K valleys, the basis functions are chosen as:

$$|\phi^\tau\rangle = \sqrt{\frac{1}{2}}(|d_{x^2-y^2}\rangle + i\tau|d_{xy}\rangle) \quad (9)$$

or

$$|\phi^\tau\rangle = |d_{z^2}\rangle$$

The resulting energy level at K or -K valley can be defined as:

$$E^\tau = \langle \phi^\tau | \hat{H}_{SOC}^0 | \phi^\tau \rangle \quad (10)$$

where the subscript $\tau = \pm 1$ refers to valley index. If $d_{x^2-y^2}+d_{xy}$ orbitals dominate -K and K valleys, the valley splitting $|\Delta E|$ is given by:

$$|\Delta E| = |E^K - E^{-K}| = 4\alpha \quad (11)$$

If the -K and K valleys are mainly from d_{z^2} orbitals, the valley splitting $|\Delta E|$ is expressed as:

$$|\Delta E| = |E^K - E^{-K}| = 0 \quad (12)$$

Clearly, these results agree with the difference of the valley polarizations in the conduction and valence bands with different U from DFT calculations.

Subsequently, the in-plane MA is assumed to investigate electronic properties of VSi_2P_4 monolayer as a function of U . The total energy band gap along with those at -K/K point and the valley splitting for both valence and conduction bands as a function of U are plotted in Figure 5, and the representative energy band structures are shown in FIG.6 of ESI. With increasing U , the gap decreases, and then increases. In considered U range, the gaps at -K and K points coincide completely, and the valley splitting is always zero. These mean that no spontaneous valley polarization and QAH phase can appear in VSi_2P_4 . For $d_{x^2-y^2}+d_{xy}$ -dominated -K and K valley, $\Delta E = 4\alpha\cos\theta$ ⁴² with general magnetization orientation, where $\theta=0/90^\circ$ means out-of-plane/in-plane direction. For in-plane one, the valley splitting of VSi_2P_4 become zero. Thus, VSiGeN_4 monolayer is a common magnetic semiconductor (CMS).

According to the MAE and electronic structure discussed above, the intrinsic phase diagram of VSi_2P_4 monolayer is shown in Figure 6, and the electronic state includes CMS, FV and VQAH. For VA_2Z_4 , the $U=3$ eV has been widely used in previous calculations^{9,15-21}. The phase diagram shows that VSi_2P_4 intrinsically is not a FV material. However, the FV states can be easily achieved by external magnetic field due to small MAE. The external magnetic field to overcome energy barrier from in-plane to out-of-plane as a function of U is plotted in Figure 7. At $U=3$ eV, the energy barrier is equivalent to applying a external magnetic field of around 0.03-0.06 T. Although the U can not be directly tuned in experiment, it can be regulated equivalently by strain, which has been confirmed in monolayer RuBr_2 ¹¹. For a given material, the correlation strength should be fixed. Even though VSi_2P_4 dose not belong to special QAH phase in the phase diagram, the QAH state can be realized by strain or external magnetic field and strain. Strain-induce QAH states have been predicted in many 2D systems^{11,19,21,43}.

V. CONCLUSION

In summary, we have demonstrated that the inclusion of MSA can result in a different phase diagram in VSi_2P_4 . For fixed out-of-plane situation, the VQAH state can be observed between two HVM states, which is related with twice sign-reversible Berry curvature and twice band inversions of $d_{xy}+d_{x^2-y^2}$ and d_{z^2} orbitals at -K or K valleys. For assumed in-plane situation, VSi_2P_4 is a CMS, and shows no spontaneous valley polarization. At representative $U=3$ eV^{9,15-21}, VSi_2P_4 is a CMS, which is different from previous FV material with only considering MCA energy^{9,17}. However, spontaneous valley polarization can be realized by small external magnetic field. It is possible to achieve QAH state in VSi_2P_4 by strain or external magnetic field and strain. Our works can deepen our understanding of MSA in the V-based 2D MA_2Z_4 family materials.

ACKNOWLEDGMENTS

This work is supported by the Natural Science Basis Research Plan in Shaanxi Province of China (2021JM-

456) and the National Natural Science Foundation of China (No. 12104130). We are grateful to Shanxi Supercomputing Center of China, and the calculations were performed on TianHe-2.

-
- ¹ N. D. Mermin and H. Wagner, *Phys. Rev. Lett.* **17**, 1133 (1966).
- ² B. Huang, G. Clark, E. Navarro-Moratalla, D. R. Klein, R. Cheng, K. L. Seyler, D. Zhong, E. Schmidgall, M. A. McGuire, D. H. Cobden, W. Yao, D. Xiao, P. Jarillo-Herrero and X. Xu, *Nature (London)* **546**, 270 (2017).
- ³ C. Gong, L. Li, Z. Li, H. Ji, A. Stern, Y. Xia, T. Cao, W. Bao, C. Wang, Y. Wang, Z. Q. Qiu, R. J. Cava, S. G. Louie, J. Xia and X. Zhang, *Nature (London)* **546**, 265 (2017).
- ⁴ Z. Wang, M. Gibertini, D. Dumcenco, T. Taniguchi, K. Watanabe, E. Giannini, and A. F. Morpurgo, *Nat. Nanotechnol.* **14**, 1116 (2019).
- ⁵ D. R. Klein, D. MacNeill, Q. Song, D. T. Larson, S. Fang, M. Xu, R. A. Ribeiro, P. C. Canfield, E. Kaxiras, R. Comin, and J. H. Pablo, *Nat. Phys.* **15**, 1255 (2019).
- ⁶ J. L. Lado and J. Fernández-Rossier, *2D Mater.* **4**, 035002 (2017).
- ⁷ J. M. Kosterlitz and D. J. Thouless, *J. Phys. C. Solid State Phys.* **6**, 1181 (1973).
- ⁸ X. Liu, H. C. Hsu, and C. X. Liu, *Phys. Rev. Lett.* **111**, 086802 (2013).
- ⁹ S. Li, Q. Q. Wang, C. M. Zhang, P. Guo and S. A. Yang, *Phys. Rev. B* **104**, 085149 (2021).
- ¹⁰ S. D. Guo, J. X. Zhu, M. Y. Yin and B. G. Liu, *Phys. Rev. B* **105**, 104416 (2022).
- ¹¹ S. D. Guo, W. Q. Mu and B. G. Liu, *2D Mater.* **9**, 035011 (2022).
- ¹² X. B. Lu, R. X. Fei, L. H. Zhu and L. Yang, *Nat. Commun.* **11**, 4724 (2020).
- ¹³ K. Yang, G. Y. Wang, L. Liu, D. Lu and H. Wu, *Phys. Rev. B* **104**, 144416 (2021).
- ¹⁴ Y. L. Hong, Z. B. Liu, L. Wang T. Y. Zhou, W. Ma, C. Xu, S. Feng, L. Chen, M. L. Chen, D. M. Sun, X. Q. Chen, H. M. Cheng and W. C. Ren, *Science* **369**, 670 (2020).
- ¹⁵ L. Wang, Y. Shi, M. Liu, A. Zhang, Y.-L. Hong, R. Li, Q. Gao, M. Chen, W. Ren, H.-M. Cheng, Y. Li, and X.-Q. Chen, *Nature Communications* **12**, 2361 (2021).
- ¹⁶ Q. R. Cui, Y. M. Zhu, J. H. Liang, P. Cui and H. X. Yang, *Phys. Rev. B* **103**, 085421 (2021).
- ¹⁷ X. Y. Feng, X. L. Xu, Z. L. He, R. Peng, Y. Dai, B. B. Huang and Y. D. Ma, *Phys. Rev. B* **104**, 075421 (2021).
- ¹⁸ D. Dey, A. Ray and L. P. Yu, *Phys. Rev. Materials* **6**, L061002 (2022).
- ¹⁹ Y. L. Wang and Y. Ding, *Appl. Phys. Lett.* **119**, 193101 (2021).
- ²⁰ X. Zhou, R. Zhang, Z. Zhang, W. Feng, Y. Mokrousov and Y. Yao, *npj Comput. Mater.* **7**, 160 (2021).
- ²¹ S. D. Guo, W. Q. Mu, J. H. Wang, Y. X. Yang, B. Wang and Y. S. Ang, arXiv:2205.07012 (2022).
- ²² P. Hohenberg and W. Kohn, *Phys. Rev.* **136**, B864 (1964); W. Kohn and L. J. Sham, *Phys. Rev.* **140**, A1133 (1965).
- ²³ G. Kresse, *J. Non-Cryst. Solids* **193**, 222 (1995).
- ²⁴ G. Kresse and J. Furthmüller, *Comput. Mater. Sci.* **6**, **15** (1996).
- ²⁵ G. Kresse and D. Joubert, *Phys. Rev. B* **59**, 1758 (1999).
- ²⁶ J. P. Perdew, K. Burke and M. Ernzerhof, *Phys. Rev. Lett.* **77**, 3865 (1996).
- ²⁷ S. L. Dudarev, G. A. Botton, S. Y. Savrasov, C. J. Humphreys and A. P. Sutton, *Phys. Rev. B* **57**, 1505 (1998).
- ²⁸ T. Fukui, Y. Hatsugai and H. Suzuki, *J. Phys. Soc. Japan.* **74**, 1674 (2005).
- ²⁹ H. J. Kim, <https://github.com/Infant83/VASPBERRY>, (2018).
- ³⁰ H. J. Kim, C. Li, J. Feng, J.-H. Cho, and Z. Zhang, *Phys. Rev. B* **93**, 041404(R) (2016).
- ³¹ A. A. Mostofia, J. R. Yatesb, G. Pizzif, Y.-S. Lee, I. Souza, D. Vanderbilt and N. Marzari, *Comput. Phys. Commun.* **185**, 2309 (2014).
- ³² Q. Wu, S. Zhang, H. F. Song, M. Troyer and A. A. Soluyanov, *Comput. Phys. Commun.* **224**, 405 (2018).
- ³³ J. B. Goodenough, *Phys. Rev.* **100**, 564 (1955).
- ³⁴ J. Kanamori, *J. Phys. Chem. Solid* **10**, 87 (1959).
- ³⁵ K. Sheng, Q. Chen, H. K. Yuan and Z. Y. Wang, *Phys. Rev. B* **105**, 075304 (2022).
- ³⁶ J. L. Lado and J. Fernández-Rossier, *2D Mater.* **4**, 035002 (2017).
- ³⁷ P. Jiang, L. Kang, Y.-L. Li, X. Zheng, Z. Zeng, and S. Sanvito, *Phys. Rev. B* **104**, 035430 (2021).
- ³⁸ S. Zhang, R. Xu, W. Duan, and X. Zou, *Adv. Funct. Mater.* **29**, 1808380 (2019).
- ³⁹ H. Hu, W. Y. Tong, Y. H. Shen, X. Wan, and C. G. Duan, *npj Comput. Mater.* **6**, 129 (2020).
- ⁴⁰ W. Y. Tong, S. J. Gong, X. Wan, and C. G. Duan, *Nat. Commun.* **7**, 13612 (2016).
- ⁴¹ P. Zhao, Y. Dai, H. Wang, B. B. Huang and Y. D. Ma, *ChemPhysMater*, **1**, 56 (2022).
- ⁴² R. Li, J. W. Jiang, W. B. Mi and H. L. Bai, *Nanoscale* **13**, 14807 (2021).
- ⁴³ H. Huan, Y. Xue, B. Zhao, G. Y. Gao, H. R. Bao and Z. Q. Yang, *Phys. Rev. B* **104**, 165427 (2021).